Chemical Physics Letters 699 (2018) 155–161

Contents lists available at ScienceDirect

Chemical Physics Letters

journal homepage: www.elsevier.com/locate/cplett

Research paper

On the fly quantum dynamics of electronic and nuclear wave packets

Ksenia G. Komarova [a,*], F. Remacle [a,b], R.D. Levine [a,c]

[a] The Fritz Haber Center for Molecular Dynamics and Institute of Chemistry, The Hebrew University of Jerusalem, Jerusalem 91904, Israel
[b] Theoretical Physical Chemistry, UR MolSys B6c, University of Liège, B4000 Liège, Belgium
[c] Department of Molecular and Medical Pharmacology, David Geffen School of Medicine and Department of Chemistry and Biochemistry, University of California, Los Angeles, CA 90095, USA

ARTICLE INFO

Article history:
Received 9 January 2018
In final form 22 March 2018
Available online 26 March 2018

Keywords:
Post Born-Oppenheimer
Grid computations
Discrete variable representations
Non-adiabatic coupling
Finite difference approximations

ABSTRACT

Multielectronic states quantum dynamics on a grid is described in a manner motivated by on the fly classical trajectory computations. Non stationary electronic states are prepared by a few cycle laser pulse. The nuclei respond and begin moving. We solve the time dependent Schrödinger equation for the electronic and nuclear dynamics for excitation from the ground electronic state. A satisfactory accuracy is possible using a localized description on a discrete grid. This enables computing on the fly for both the nuclear and electronic dynamics including non-adiabatic couplings. Attosecond dynamics in LiH is used as an example.

1. Introduction

Computing classical trajectories for the motion of the atoms in a molecular system clearly illustrates the advantages of computing on the fly. Accurate quantum chemical computations of the electronic structure (potential, dipole and non Born-Oppenheimer coupling terms) are required only at those configurations of the atoms that are reached by the system as it moves in time. Such computations are possible but are typically time consuming and so are the bottleneck in computing the dynamics. This is much more so for the systems with non-trivial ultrafast photo-chemical dynamics that span several electronic states and where one needs to include nonadiabatic coupling terms [1–3]. It is therefore of interest to make as few such quantum chemical computations as are essential. Computing only for configurations accessed by the system is the key in the method applied to classical trajectories. We here seek to mimic such an advantage for quantum dynamics.

In the recent developments of the on-the-fly trajectory guided basis function or multi configurational time-dependent Hartree approaches for multi-state coupled electron-nuclear dynamics [4–6] the choice of the basis functions is responsible for the localized treatment of the problem. It can be either the frozen-width Gaussian basis functions, or DVR-representations for which one can evaluate the momentum or kinetic terms explicitly but special care should be taken for the potential. Here we propose an alternative approach. We focus on a localized form of the Hamiltonian that allows for a bounded propagation that is consistent with propagation by the non-local Fourier method [7] on the grid of nuclear coordinates. The localization is achieved by the well-known finite difference approximation. As an example we describe multi-state dynamics in the LiH diatomic molecule. The structure of the Hamiltonian that we use provides insight on extending the approach to multidimensional grid. Specifically the equation of motion of the amplitude at a particular grid point, see Eq. (3) below, will remain linear and bounded because the Hamiltonian Fig. 2, will only couple near neighbors in each direction. As in other approaches on the fly, the bottleneck remains computing the potential at a multitude of grid points.

A quantal description of a molecular system of several coupled electronic states requires solving the time dependent Schrödinger equation, a subject of recent interest [4,5,8–13]. A wave function is not quite analogous to a classical trajectory. This is particularly so when one aims to describe an excitation from an initial state. We typically choose a stationary initial state so that the change is due to the perturbation. Such an initial state is usually delocalized in the coordinates of the atoms. This is quite different from the initial conditions of a classical trajectory that initiates at a particular configuration. Representing the initial wave packet dynamics by an ensemble of these classical trajectories is limited as each one moves independently of the other. Lost thereby is the effect of the non-locality (meaning coherence between amplitudes on adjacent grid points) of the momentum and kinetic operators on the propagation (see Appendix A for the short

* Corresponding author.
E-mail address: kgvladi@fh.huji.ac.il (K.G. Komarova).

https://doi.org/10.1016/j.cplett.2018.03.050
0009-2614/

discussion on the subject). In the powerful method describing the motion of atoms on a discrete grid [7,14–17] the kinetic energy is computed by transforming the wave function to the momentum representation where the quantum mechanical kinetic energy operator is just a multiplication. Then one transforms back to the grid in coordinate space. One need not transform to momentum space. Instead one can use a very many term finite difference expansion to compute the kinetic energy purely in coordinate space [14]. Either procedure yields a benchmark result that for a dense grid is numerically practically exact. Both techniques are very non local with a given point on the coordinate grid being coupled to many other points.

Our aims are therefore three fold. (i) To compute the kinetic energy in as local a manner as is realistic for the desired numerical accuracy. (ii) To apply an on the fly approach to a delocalized initial state. (iii) To do the above for a system evolving coherently on several electronic states. We chose the well-studied case of LiH [18,19] that has significant nonadiabatic couplings (Fig. 1), and where the successive excited electronic states alternate in the character of the binding.

There is an important fourth point that we just allude to, namely the polyatomic case. As we shall show in our approach the atoms move under the combined influence of the familiar Born Oppenheimer potential plus the vector potential [1–3] due to the coupling of different electronic states. So also for polyatomic motion one needs to sample a rather restricted range of motions of the atoms.

2. Localizing the Hamiltonian by the finite difference method

To compute the kinetic energy using a small number of grid points we here use a truncated expression for the kinetic energy. In the case of multiple degrees of freedom one can apply efficient algorithms of 3D-finite difference schemes [20] for the grid in Cartesian coordinates. For a single nuclear coordinate, as is the case here, the kinetic energy operator couples a grid point i only to its near neighbor, one on each side, grid-points that are a distance a apart:

$$-\frac{\hbar^2}{2m}\frac{\partial^2}{\partial x^2}f(x_i) \cong -\frac{\hbar^2}{2ma^2}(f(x_i+a)-2f(x_i)+f(x_i-a)) = -\frac{\hbar^2}{2ma^2}(f(x_{i+1})-2f(x_i)+f(x_{i-1})) \quad (1)$$

m is the reduced mass. To be reasonably accurate the spectrum of the finite difference operator $\left(\hbar^2/2ma^2\right)2cos(ka)$ needs to approximate well the spectrum of the kinetic energy $\left(\hbar^2/2m\right)k^2$.

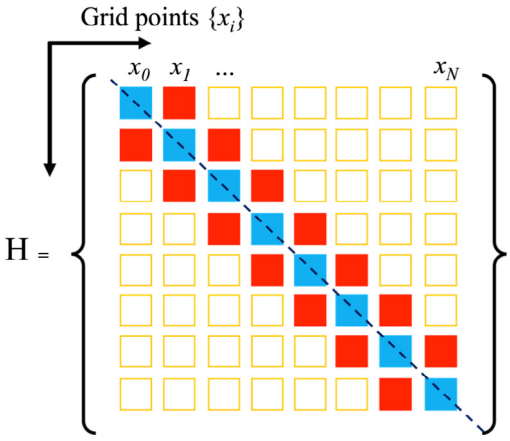

Fig. 2. Block tri-diagonal form of the Hamiltonian in the case of 3-point finite difference approximation defined on a discrete grid of N points $\{x_0, x_1, \ldots, x_N\}$ for the nuclear coordinate x. The diagonal blocks (blue boxes) consist of operators that are local in the grid coordinates; non-local operators (red boxes) couple only neighbor grid points. With such a Hamiltonian we can compute a wave function for multi electronic states on the fly. (For interpretation of the references to colour in this figure legend, the reader is referred to the web version of this article.)

Therefore, in terms of a characteristic momentum the grid spacing needs to satisfy $ka < 1$. But this is necessary in any case if we are to have enough grid points per de Broglie wave length. So already the near neighbor approximation is quite realistic (see Appendix, Fig. A1), and suffices for many purposes. A next near neighbor approximation, defined in the Appendix (see Eq. (A2)), retains two grid points on either side of a given point. When $ka < 1$such a five point approximation is essentially exact (see Fig. A1). Corresponding to Eq. (1) the momentum is given (to order a^2)

$$-i\hbar\frac{\partial}{\partial x}f(x_i) = -\frac{i\hbar}{2a}(f(x_{i+1})-f(x_{i-1})) \quad (2)$$

As it should the momentum has a direction along the grid.

When an ultra short laser pulse is switched on, the several electronic states whose energies are within the wide spectrum range of the pulse can be populated at each grid point. The time-dependent wave function is here described in the basis of adiabatic states, for which the diagonal and off-diagonal terms of the Hamiltonian can be computed using quantum chemical (QC) multi state methodologies at each particular value of the internuclear distance that corresponds to a given grid point. We propagate a coherent superposition of electronic states with an amplitude for the nuclear motion on the grid on each electronic state. We extend

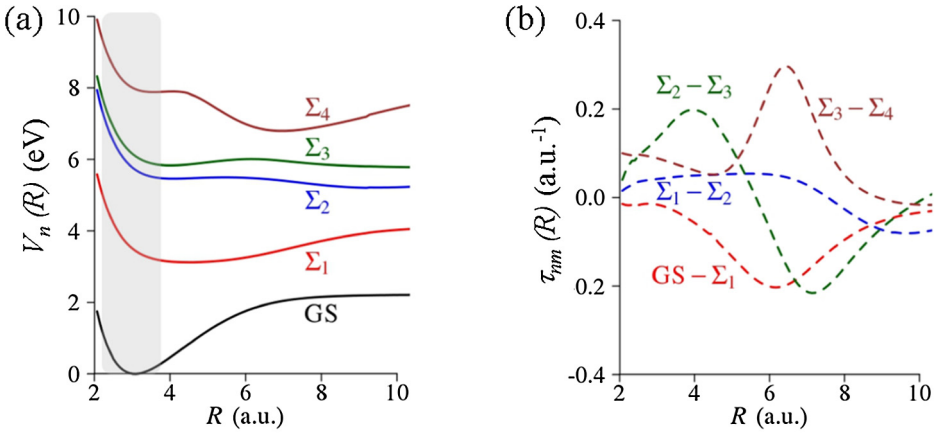

Fig. 1. Adiabatic potentials (a) and non-adiabatic coupling terms (b) in LiH as a function of the internuclear distance R calculated at the CASSCF level. See Appendix B for the computational details.

the range of the grid as required by the dynamics of the nuclear wave packets on different electronic states.

The Hamiltonian including non-adiabatic coupling can be written using the generalized momentum $\mathcal{P}$ introduced by Smith [1] as $H = (\mathcal{P}^2/2m) + V$. $\mathcal{P}$ is the sum of the momentum of the nuclei and the momentum type terms introduced by the non-adiabatic coupling [2,3]. On the grid, the time-dependent Schrödinger equation for the amplitude, C_{ni}, of the electronic state n at the grid point i (internuclear distance x_i), using a near neighbor kinetic energy operator, Eq. (1) and the two point difference for the momentum, Eq. (2), is:

$$i\hbar\frac{dC_{ni}}{dt} = \left(T_d + V_{nn}(i) + (Y_{nn}(i)/2m) - E(t)\mu_{nn}(i)\right)C_{ni} + T_{nd}C_{ni-1} + T_{nd}C_{ni+1} - \sum_{k\neq n}\left(E(t)\mu_{nk}(i)C_{ki} - \frac{\hbar}{2ma}\tau_{nk}(i)(C_{ki-1} - C_{ki+1}) + \frac{1}{2m}Y_{nk}(i)C_{ki}\right) \quad (3)$$

where the index k is the index of all the accessible electronic states, and $\{i-1, i+1\}$ are the indices of the grid points neighboring i. The terms of the Hamiltonian diagonal in the electronic index include the kinetic energy coupling constants, see Eq. (1), that are not dependent neither on the grid nor on electronic index, $T_d = \hbar^2/ma^2$ and $T_{nd} = -\hbar^2/2ma^2$. The notation non-diagonal on the kinetic energy, T_{nd}, is to emphasize that this operator, which is diagonal in the electronic state index, shifts the wave function along the grid whereas the diagonal counterpart, T_d, only shifts the phase. The adiabatic electronic energy of state n at the internuclear distance x_i, acts as a potential $V_{nn}(i)$ at the grid point i. Another term that is diagonal in the electronic state index is the coupling to the laser field, $E(t)$, due to non-zero permanent dipole moment $\mu_{nn}(i)$ of the electronic state. Off-diagonal matrix elements of the Hamiltonian couple different electronic states and thus leads to changes in the amplitudes of the coupled states. These consist of the coupling to the laser field due to the transition dipoles between different electronic states $\mu_{nk}(i)$ and non-adiabatic coupling terms. The non-adiabatic couplings for the electronic states n and k at grid point i are given by:

$$\tau_{nk}(i) = \hbar\langle\psi_n|\tfrac{\partial}{\partial x}\psi_k\rangle_{x=x_i}$$
$$Y_{nk}(i) = \hbar^2\langle\psi_n\left|\tfrac{\partial^2}{\partial x^2}\psi_k\right\rangle_{x=x_i} \quad (4)$$

The site-dependent coupling term $(\hbar/ma)\tau_{nk}(i)$ acts just like a non-diagonal kinetic energy in the sense that it shifts population from site i to its two near neighbors. The magnitude of this coupling differs for different electronic states. Unlike T_{nd}, this term is not diagonal in the electronic states. It shifts amplitude to adjacent grid points and to all electronic states.

A key point about Eq. (3) is that the Hamiltonian has localized coupling between the points on the grid: C_{ni} is coupled only to C_{ni-1} and C_{ni+1}. In other words, the Hamiltonian is block tridiagonal as shown in Fig. 2. The size of each block is the number of accessed electronic states, typically much fewer than the number of grid points. Each block on the diagonal, blue in the figure, is made of the operators local in the nuclear coordinate i, see Eq. (2). A diagonal block is coupled to its two near neighbors, shown in red.

3. Coherent quantum dynamics on the fly

In this Letter we discuss computing on the fly towards accurate quantum dynamics of coherent electronic and nuclear wave packets. Technically we start from a wave function and QC computations of matrix elements of the Hamiltonian defined over a localized small region of the grid. In principle it can be three grid points or even just one point. Using a Hamiltonian that couples only near neighbors, see Fig. 2, we can, at each time step, increase the span of the region by adding just one grid point to each side of the grid as shown in Fig. A2 of the Appendix.

The ability to compute electronic structure in parallel suggests starting from a larger region on the grid and also adding a small but finite number of points at each expansion. This is because our physical initial conditions are that prior to the onset of the laser pulse the molecule is in its ground state. We therefore confine the initial grid to a small relevant range about the equilibrium position of the ground state potential well (Fig. 3a). This neglects the far tails of the ground state vibrational wave function. The pumping by the laser should be switched on only after the initial localized wave function is propagated for enough time that it spreads to a reasonable extent. As the wave packet propagates we increase the dimension of the grid over which the matrix elements of the Hamiltonian are needed. We expand the grid only if the population at the edge is large. Thereby we make fewer extensions of the grid but each extension span more than one grid point.

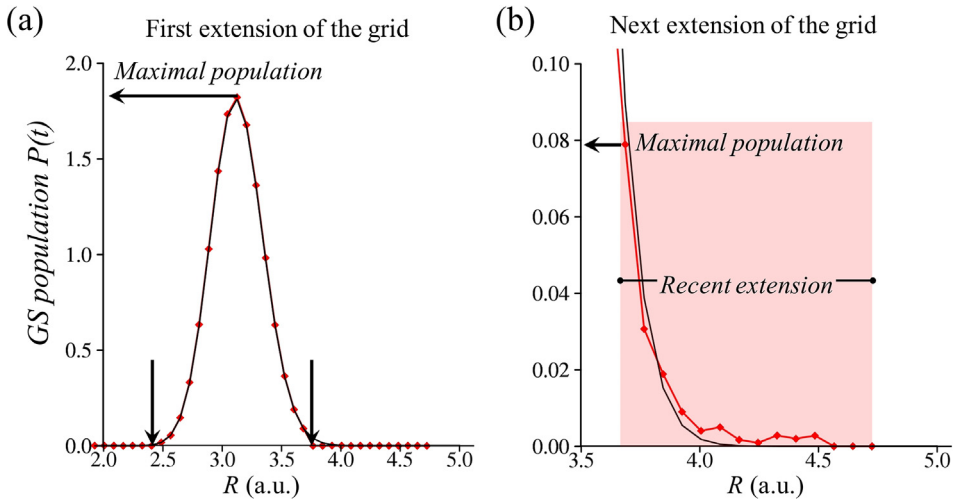

Fig. 3. (a) Initial ground state population profile for the restricted grid of the on-the-fly computation (red line with diamonds) compare to the 512 point full grid (black line). The population at the red points to either side of the two arrows is set to zero. (b) The tail of the profiles, black: full grid; red line with diamonds: on the fly, after propagation in the region of the first extension (area shaded in red). The threshold is defined relative to the maximum population over the grid points of the most recent extension (13 grid points, 1 a.u. from the edge). (For interpretation of the references to colour in this figure legend, the reader is referred to the web version of this article.)

The value of the population at the edge at which we expand is determined by comparing the ratio of the population at the edge to the maximal value. Once this fraction ξ, is larger than the threshold value, here 0.05, we expand. In general the population on a given electronic state can have more than one maximum. Before the first extension, the maximal population is defined over all set of grid points (Fig. 3a). During all the subsequent extensions of the grid the maximal population is taken over the region of the most recent extension. The first such extension is shown in Fig. 3b. In the direction towards dissociation the excited state potentials are shallow. In this case, we take the range of the extension to be 1 a.u. corresponding to the width of the initial GS wavepacket. This is because the wavepackets of the excited states pumped by the ultrashort pulse from the ground state have initially the same width. We extend the grid towards the repulsive potential by 0.6 a.u. due to steep walls of the potentials at short Li-H distances. This extension to the left is needed only once because the wavepackets on each excited state move out.

Due to the localized form of the momentum and kinetic energy neglecting the tails of the wave packet affects only coefficients at the edge of the grid. The error is on the order of the values of the amplitudes multiplied by the coupling constants ($\hbar\tau/2ma$ or $\hbar^2/2ma^2$ for momentum and kinetic terms, respectively) at the points not included in the current grid. Amplitudes below the threshold can be reflected from the current edge of the grid and this is the source of the error. As a compensating error one can apply an absorbing potential with renormalization of the amplitude in that channel. Each time we extend the grid we compute the matrix elements only at the additional points and restart the dynamics from previous coefficients on the new, larger grid. Essential details are provided in Appendix C. Quantum chemical computations are, by far, the most time consuming step. As in the case of the computations using initially large grids because matrix elements at each grid point are independent from the others one benefits from running QC computations in parallel. In the present approach, one can optimize between the number of expansions of the grid during the dynamics, the number of grid points added per each expansion and the number of available computational nodes.

Our computational example is multi-state electron-nuclear dynamics in LiH upon interaction of the ground state with a short, one cycle IR 800 nm pulse [19]. The electric field is polarized along the molecular axis so that only the manifold of Σ states is excited. Details regarding quantum chemical calculations can be found in the appendices. The pulse strength is kept low enough to preclude any significant ionization: the maximal amplitude of the field was set to 0.04 a.u. which corresponds to the intensity of $5.61 \cdot 10^{13}$ W/cm^2. We thus need to consider only ground state (GS) and 4 excited states of Σ symmetry, all of which lie below the first ionization potential in LiH. Extension to the basis set of both neutral and ionic electronic states is possible [21]. When adding new electronic states to the basis the performance of the finite difference approximation of the kinetic energy for the lower states remains the same because the kinetic energy terms are diagonal in the electronic state index.

We define an initial localized wave packet on the ground state over 16 grid points about the equilibrium position of the ground state, see Fig. 3a. Such a wave function approximates the actual ground state apart from its wings. After the first time step we extend the grid at the two edges so that it spans the [1.92, 4.72] range of distances, comprising 36 grid points (Fig. 4b). For such an initial state we can switch the laser on without a special delay. Both population and dipole dynamics are described with a high accuracy for such an approximate initial nuclear wave packet (Fig. 4) as compared to FT computations initiated on the stationary ground state defined on a large grid of 512 points (see Fig. A3 for the relative errors). The time-dependent dipole is more sensitive to the accuracy of the approximation because it is determined by the coherence of different electronic states.

Extensions of the grid will be needed several times as the dynamics unfold. For the current 5 adiabatic state basis, we have two bound states (GS and Σ_1) and 3 almost repulsive potentials (Σ_2, Σ_3 and Σ_4) as shown in Fig. 1a. The first extension is needed after one time step due to the motion on the ground state, see Fig. 4b. The second computation of the Hamiltonian terms at additional grid points is requested during the pulse due to the population on the Σ_4 potential that accumulates at the edge of the grid. The additional extensions and the excited states for which they

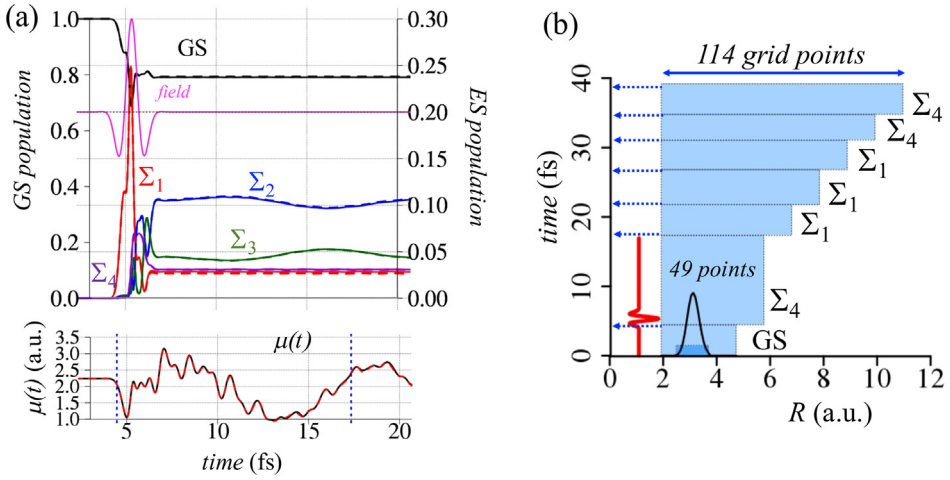

Fig. 4. (a) Top panel: Population dynamics computed for a grid of 512 points using a Fourier transform (FT) for computing the kinetic energy and momentum terms (solid lines) and on the fly computations (dashed lines) for the five lowest electronic states of LiH photoexcited by an IR 1-cycle pulse (magenta curve, not at scale). The bottom panel shows the comparison between the dipole moment computed on the fly (red dashed line) and using FT method on the initially large grid (black line). Vertical blue lines mark the time of the grid expansion. See Appendix B for details about the Hamiltonian matrix and the pulse parameters. (b) On the fly extension of the grid (region confined within light blue boxes) during first 40 fs of the electron-nuclear dynamics in LiH upon interaction with 1-cycle IR pulse shown as a red curve vs. time on the bottom left. The initial ground state (GS) wave packet (black solid line) is defined on the set of 16 points (blue bar). After the first time step an extension of 36 grid points is needed. Still during the pulse one further extension is necessary due to population of the Σ_4 around the edge of the grid. (For interpretation of the references to colour in this figure legend, the reader is referred to the web version of this article.)

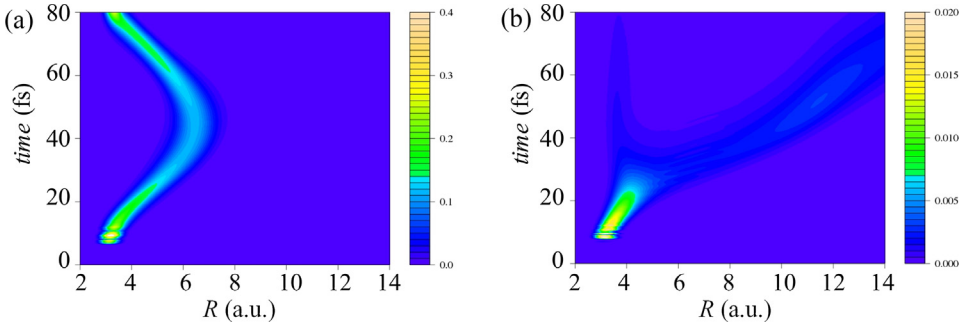

Fig. 5. Heat maps of the population of the bound Σ_1 (a) and dissociative Σ_4 (b) electronic states as a function of internuclear distance for the first 80 fs of the dynamics.

are required are shown in Fig. 4b. One can see that around 30 fs, when the wave packet of the bound Σ_1 state gets closer to the outer turning point (Fig. 5a), the extension of the grid is required because of large Σ_4-population at long distances (Fig. 5b). In the dynamical computations we continued to propagate beyond the range of internuclear distance shown below and ended up at a full grid of 512 points.

4. Conclusions

Using a Hamiltonian that only couples near neighboring grid points we implemented an on the fly approach to accurately compute the quantum dynamics of multi electronic state systems. One can propagate one grid point at a time but it is more practical to extend the grid by a finite number of grid points. We predefine the range of extension separately for each side to account the shape of the potentials and the direction of motion of the wavepackets. This is because the very time demanding quantum chemical computations can then be done in parallel at all these additional points. In more dimensions restriction of the dynamics to the relevant ranges will remain as the major saving, because computation of the Hamiltonian terms will still be the most time-consuming part.

Acknowledgements

This work is supported by the U.S. Department of Energy (DOE), Office of Science, Basic Energy Sciences (BES) under Award #DE-SC0012628 and by the Fonds de la Recherche Fondamentale Collective (T.0132.16 and J.0012.18). We benefited from our participation in the COST action CM 1405 MOLIM. We thank S. van den Wildenberg for additional computations on LiH. FR thanks Fonds National de la Recherche Scientifique (F.R.S.-F.N.R.S) for its support.

Appendix A. Quantum effects for coherent wave packets described on a grid

The essential difference between the classical and quantal treatment of the population dynamics is seen in the equation for the rate of change of the local population $n_{ki}(t)$ of the electronic state k at the grid point i.

$$\frac{dn_{ki}}{dt} = 2T_{nd}\left[Im\left(C_{ki}^{*}C_{ki-1}\right) + Im\left(C_{ki}^{*}C_{ki+1}\right)\right] + \sum_{l\neq k}(1/ma)\tau_{kl}(i)\left[Im\left(C_{ki}^{*}C_{li-1}\right) - Im\left(C_{ki}^{*}C_{li+1}\right)\right] - \sum_{l\neq k}(1/\hbar m)Y_{kl}(i)Im\left(C_{ki}^{*}C_{li}\right) \quad \text{(A1)}$$

Spreading of the wave packet along the grid within one electronic state is determined by the coherences between the amplitudes at the adjacent points of the same electronic state (first line of the Eq. (A1)). Population transfer to other electronic states l (other terms of Eq. (A1)) also depends not only on the strength of the coupling, but also on the coherences between the amplitudes of the coupled electronic states on neighboring grid points.

Appendix B. Computational details

The diagonal and off-diagonal terms of the electronic Hamiltonian for each particular grid-point were computed at the CASSCF

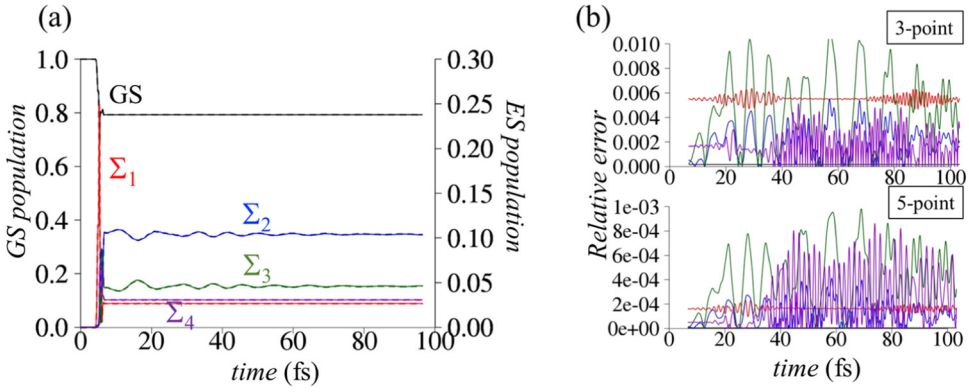

Fig. A1. (a) Population dynamics computed with a 5-point finite difference approximation (dashed lines) compared to the dynamics computed with Fourier transform (FT) method (solid lines) on precomputed potentials and couplings on a grid of 512 points (a = 0.08 a.u.). (b) Error in the populations computed with the 3-point (Eq. (1)) (b, top panel) and the 5-point (Eq. (A2)) (b, bottom panel) FD approximation with respect to the FT method. Black lines correspond to the ground state (GS) population, red to Σ_1, blue to Σ_2, green to Σ_3, violet to Σ_4. (For interpretation of the references to colour in this figure legend, the reader is referred to the web version of this article.)

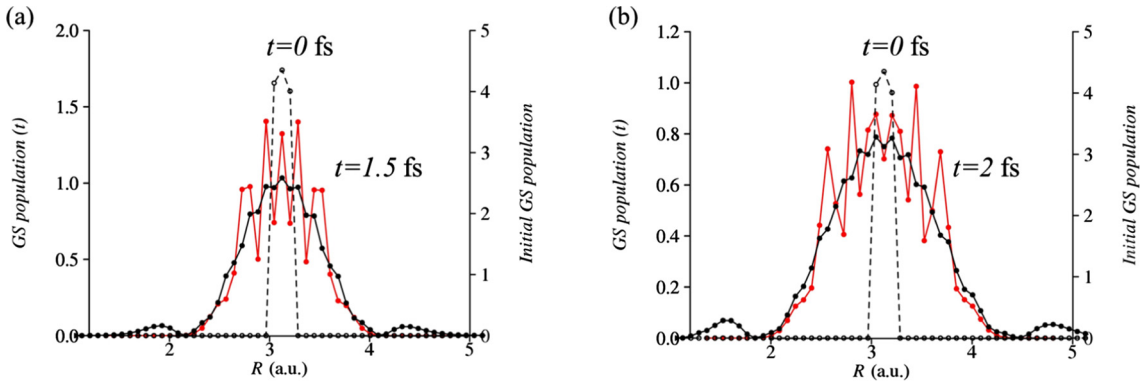

Fig. A2. Ground state population profile at different times ((a) 1.5 fs, (b) 2 fs) starting from the 3-point only wave packet (t = 0 fs, dashed line) centered at the equilibrium position of the GS. Black lines correspond to the results calculated within FT method on 512 grid points, red lines – finite difference (5-point approximation). The errors are shown in Fig. A3. The on the fly propagation is defined by a threshold ξ (see Fig. 3 of the main text) of 5% compared to a FT computation where the 512 point grid is available at all times. (For interpretation of the references to colour in this figure legend, the reader is referred to the web version of this article.)

level using the MULTI program [22] of the suite of quantum chemistry MOLPRO package [23]. State averaged wave functions of the lowest 15 electronic states of Σ symmetry were built within Gaussian 6-31+G(df, p) basis set. Configurations containing all 4 electrons in the active space of 13/7/7/2 molecular orbitals (of $\Sigma/\Pi_x/\Pi_y$ and Δ symmetry, respectively) were used. If at some grid-points the CASSCF procedure fails to converge, an automatic restart from the CASSCF wave functions on the neighboring points (±0.01 a.u.) was enabled within the same QC computation as implemented in MOLPRO package [23]. Non-adiabatic coupling terms were obtained using DDR procedure based on a finite difference scheme for the computation of the derivative of the electronic wave function using a step size of 0.01 a.u. in internal coordinates with center of mass being fixed at $R_{c.m.}$ = 0. The second order non-adiabatic coupling terms were computed using numerical derivative of the first order terms [3]. The full set of matrix elements of the Hamiltonian computed at this level of theory is in good agreement with previously published results, based on the internally contracted MRCI calculations [19,24]. For the presented case of one dimensional nuclear dynamics the QC computations are the most time consuming part: one computation is taking 20–70 min on one CPU, depending on the convergence of the CASSCF procedure. Fixed value of the extension length enables to sequentially build Hamiltonian which can be further used for different pulses scenario as the dynamics unfold (considering that the basis set of electronic states is sufficient).

The time-dependent Schrödinger equation for the amplitudes (Eq. (2) of the main text) is solved using a fourth-order Runge-Kutta method, with time step of 0.01 time a.u. and the step of the grid a = 0.08 a.u. in internal nuclear coordinate (512 grid points). For the FT computations FFTW library [25] was used for computing the discrete Fourier transform. For the on-the-fly computations a 5-point approximation,

$$-\frac{\hbar^2}{2m}\frac{\partial^2}{\partial x^2}f(x_i) = -\frac{\hbar^2}{24ma^2}\left(-f(x_{i-2}) + 16f(x_{i-1}) - 30f(x_i) + 16f(x_{i+1}) - f(x_{i+2})\right) \quad \text{(A2)}$$

was used wherever needed meaning for the momentum in the non-adiabatic coupling terms, the kinetic energy and for the derivative Y_{nk} of the non-adiabatic coupling terms. The small diagonal elements Y_{nn} are not included in the dynamical computations.

The interaction with pulse was described within dipole approximation, using explicit time profile of the electric field [18]:

$$\mathbf{E}_p(t) = (-1/c)\partial\mathbf{A}_p(t)/\partial t = = \mathbf{E}_p exp\left(-(t-t_p)^2/2\sigma_p{}^2\right)\left(cos(\omega_p t) - \frac{(t-t_p)}{\omega_p\sigma_p^2}sin(\omega_p t)\right)$$

$$\mathbf{A}_p = -\frac{\mathbf{E}_p c}{\omega_p}exp\left(-(t-t_p)^2/2\sigma_p{}^2\right)sin(\omega_p t) \quad \text{(A3)}$$

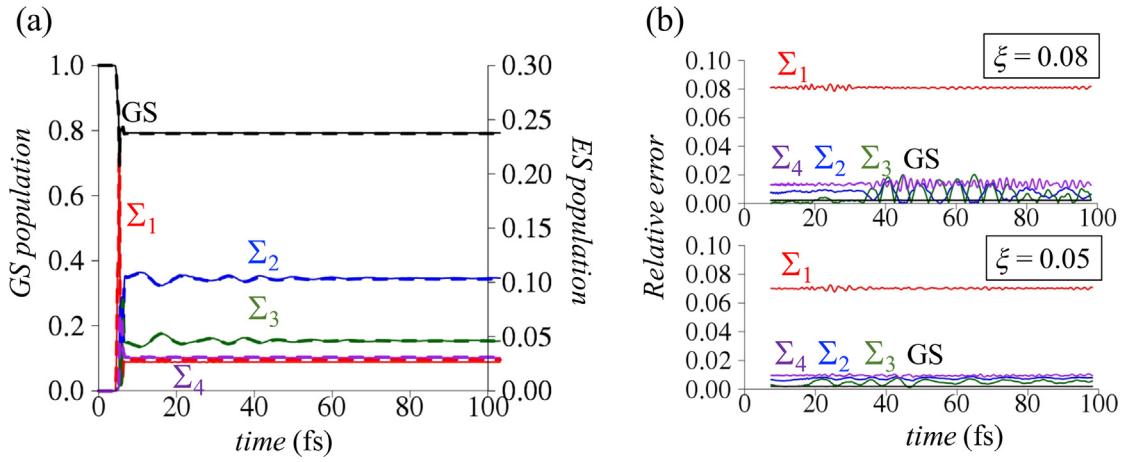

Fig. A3. (a) Population dynamics computed within on-the fly with 8% threshold in population (dashed lines) and FT method on the 512 point grid (solid lines). (b) On the fly approach errors in population dynamics relative to the population of each state for two values of the thresholds: 5% (bottom) and 8% (top). Comparison to the populations computed by FT method on the 512 grid points. The error in Σ_1 is larger primarily because the ground state wave packet hits the edge of its allowed grid when the threshold is at 5% or 8%.

where $\mathbf{E}_p(t)$ is electric field which corresponds to the vector potential $\mathbf{A}_p$. The direction of the pulse is chosen to be along the H-Li vector, $\mathbf{E}_p = |E_z^p|\mathbf{e}_z$, with amplitude $|E_z^p| = 0.04$ a.u. The frequency of the pulse ω_p was chosen to be 800 nm, with $\sigma_p = 20$ a.u. of time.

The electron-nuclear dynamics is described in terms of time-dependent population of each electronic state, defined by:

$$n_k(t) = \sum_i |C_{ki}(t)|^2 \tag{A4}$$

and the time-dependent dipole moment:

$$\mu_{tot}(t) = \sum_{n,i} |C_{ni}(t)|^2 \mu_{nn}(i) + \sum_{n \neq k,i} \left[C_{ni}^*(t) C_{ki}(t) + C_{ki}^*(t) C_{ni}(t)\right] \mu_{nk}(i) \tag{A5}$$

Initial coefficients on the ground state were defined using analytical expression of the anharmonic wave function which corresponds to the calculated GS potential ($D_e = 2.5$ eV, $\alpha = 0.615$ (a.u.)$^{-1}$, $\lambda = 27.9$, $R_e = 3.08525$ a.u.).

The quality of the results is shown in Fig. A1. The error in population dynamics for the 3-points is less than 1%, and 5-points finite difference (FD) approximation – less than 0.1% as compared to the benchmark Fourier transform (FT) computations on the same 512 point grid.

Appendix C. On the fly computation with a wider initial range of points

To mimic the classical approach, we can start with one point or three points on the grid and extend to the left and to the right at each time step. Here we also discuss an example where we trade starting with a wider initial grid with making a smaller number of grid extensions. Fig. A3 shows ground state population profile dynamics starting from a wave packet localized over three grid points. After some time steps the wave packet on the ground state represents well the result of using a full grid. Then the electronic excitation is applied.

Next we discuss wave packet on the ground state localized over 16 grid points. Such a wave function approximates the actual ground state apart from its wings. After the first time step we extend the grid at the two edges so that it spans 36 grid points. It is then a reasonable approximation to the true ground state and we can switch the laser on. Both population and dipole dynamics compare well with the FT computations, see Fig. 4. The fractional error in the computed populations vs. the benchmark Fourier transform method are shown in Fig. A3 when a non-negligible population is in the extended region. A larger error is observed for larger value of the threshold (5% vs. 8%), because a larger portion of the population is neglected. When the threshold is increased to 10% the wavepacket on the ground state is unphysically narrow leading to errors coming from the reflection of the wavepacket from the edges.

References

[1] F.T. Smith, Diabatic and adiabatic representations for atomic collision problems, Phys. Rev. 179 (1969) 111–123.
[2] A.W. Jasper, B.K. Kendrick, C.A. Mead, D.G. Trulhar, Non-born-oppenheimer chemistry: potential surfaces, couplings and dynamics, in: X. Yang, K. Liu (Eds.), Mordern Trends in Chemical Reactions Dynamics: Experiment and Theory, World Scientific, Singapore, 2004, pp. 329–391.
[3] M. Baer, Beyond Born-Oppenheimer: Electronic Nonadiabatic Coupling Terms and Conical Intersections, Wiley, Hoboken (NJ), 2006.
[4] B. Mignolet, B.F.E. Curchod, T.J. Martínez, Communication: XFAIMS—eXternal Field Ab Initio Multiple Spawning for electron-nuclear dynamics triggered by short laser pulses, J. Chem. Phys. 145 (2016) 191104.
[5] G.W. Richings, S. Habershon, Direct quantum dynamics using grid-based wave function propagation and machine-learned potential energy surfaces, J. Chem. Theory Comp. 13 (2017) 4012–4024.
[6] G.W. Richings, S. Habershon, Direct grid-based quantum dynamics on propagated diabatic potential energy surfaces, Chem. Phys. Lett. 683 (2017) 228–233.
[7] R. Kosloff, Time-dependent quantum-mechanical methods for molecular dynamics, J. Phys. Chem. 92 (1988) 2087–2100.
[8] M. Nisoli, P. Decleva, F. Calegari, A. Palacios, F. Martín, Attosecond electron dynamics in molecules, Chem. Rev. 117 (2017) 10760–10825.
[9] M. Uwe, Wavepacket dynamics and the multi-configurational time-dependent Hartree approach, J. Phys.: Condensed Matter 29 (2017) 253001.
[10] S.M. Greene, V.S. Batista, Tensor-train split-operator Fourier transform (TT-SOFT) method: multidimensional nonadiabatic quantum dynamics, J. Chem. Theory Comput. (2017).
[11] Y. Ide, T. Kato, K. Yamanouchi, Non-Born–Oppenheimer molecular wave functions of H2 by extended multi-configuration time-dependent Hartree-Fock method, Chem. Phys. Lett. 595–596 (2014) 180–184.
[12] A. Sisto, D.R. Glowacki, T.J. Martinez, Ab initio nonadiabatic dynamics of multichromophore complexes: a scalable graphical-processing-unit-accelerated exciton framework, Acc. Chem. Res. 47 (2014) 2857–2866.
[13] X. Li, J.C. Tully, H.B. Schlegel, M.J. Frisch, Ab initio Ehrenfest dynamics, J. Chem. Phys. 123 (2005) 084106.
[14] D.J. Tannor, Introduction to Quantum Mechanics. A Time-Dependent Perspective, University Science Book, Sausalito, 2007.
[15] R. Kosloff, Propagation methods for quantum molecular dynamics, Ann. Rev. Phys. Chem. 45 (1994) 145–178.
[16] J.V. Lill, G.A. Parker, J.C. Light, The discrete variable–finite basis approach to quantum scattering, J. Chem. Phys. 85 (1986) 900–910.
[17] D.T. Colbert, W.H. Miller, A novel discrete variable representation for quantum mechanical reactive scattering via the S-matrix Kohn method, J. Chem. Phys. 96 (1992) 1982–1991.
[18] A. Nikodem, R.D. Levine, F. Remacle, Quantum nuclear dynamics pumped and probed by ultrafast polarization controlled steering of a coherent electronic state in LiH, J. Phys. Chem. A (2016).
[19] A. Nikodem, R.D. Levine, F. Remacle, Spatial and temporal control of populations, branching ratios, and electronic coherences in LiH by a single one-cycle infrared pulse, Phys. Rev. A 95 (2017) 053404.
[20] J.D. Hoffman, Numerical Methods for Engineers and Scientists, Marcel Dekker, Basel, 2001.
[21] B. Mignolet, R.D. Levine, F. Remacle, Control of electronic dynamics visualized by angularly resolved photoelectron spectra: a dynamical simulation with an IR pump and XUV attosecond-pulse-train probe, Phys. Rev. A 89 (2014) 021403.
[22] P.J. Knowles, H.-J. Werner, An efficient second-order MC SCF method for long configuration expansions, Chem. Phys. Lett. 115 (1985) 259–267.
[23] H.-J. Werner, P.J. Knowles, G. Knizia, F.R. Manby, M. Schutz, MOLPRO, a package of ab initio programs, 2015.
[24] F. Holka, P.G. Szalay, J. Fremont, M. Rey, K.A. Peterson, V.G. Tyuterev, Accurate ab initio determination of the adiabatic potential energy function and the Born-Oppenheimer breakdown corrections for the electronic ground state of LiH isotopologues, J. Chem. Phys. 134 (2011) 094306.
[25] M. Frigo, S.G. Johnson, The design and Implementation of FFTW3, Proc. IEEE 93 (2005) 216–231.